Associations of Amyloid Deposition and FDG Uptake in Aging and Cognitively Impaired Elders With and Without Moderate to Severe Periventricular White Matter Hyperintensities

Katherine Zukotynski[1,2], Vincent Gaudet[3], Philip Kuo[4], Sabrina Adamo[1], Maged Goubran[1], Christopher J.M. Scott[1], Christian Bocti[5], Michael Borrie[6], Howard Chertkow[7], Richard Frayne[8], Robert Hsiung[9], Robert LaForce[10], Michael Noseworthy[2], Frank S. Prato[11], Demetrios Sahlas[2], Eric E. Smith[8], Vesna Sossi[9], Alexander Thiel[7], Jean-Paul Soucy[12], Jean-Claude Tardif[13], Sandra E. Black[1]

[1]Sunnybrook Research Institute, [2]McMaster University, [3]University of Waterloo, [4]University of Arizona, [5]Université de Sherbrooke, [6]Western University, [7]Jewish General Hospital, [8]Hotchkiss Brain Institute, [9]University of British Columbia, [10]Université Laval, [11]Lawson Health Research Institute, [12]Montreal Neurological Institute, [13]Montreal Heart Institute

STUDY PURPOSE

To assess associations of amyloid deposition and FDG uptake in subjects with minimal versus moderate-severe periventricular white matter hyperintensity (pvWMH) using ^{18}F-Florbetapir and ^{18}F-FDG PET

BACKGROUND

- Machine Learning (ML) refers to computational tools that are trained using data
- Random forests (RF) are a type of supervised ML that trains a set (forest) of decision trees
- K-means clustering is an unsupervised ML algorithm that groups similar data points
- Both RFs and K-means clustering are simple, classical ML techniques

METHODS

- Fifty-seven participants with mild cognitive impairment (MCI), early Alzheimer Disease (AD) or transient ischemic events (MMSE score > 20) and severe pvWMH (Fazekas score = 3) recruited from memory (38) and stroke (19) clinics
- Each participant had a ^{18}F-Florbetapir PET (clinical read: 22 positive, 35 negative for amyloid deposition); fifty-five had ^{18}F-FDG PET (3 positive, 52 negative); twenty-five had 2-year follow-up ^{18}F-Florbetapir PET
- A matched cohort of 57 patients with both ^{18}F-Florbetapir (28 positive, 29 negative) and ^{18}F-FDG (2 positive, 55 negative) taken from ADNI
- We requested permission from ADNI to use their ADNI2 PET technical manual as our own, which we distributed to all of our participating sites
- PET images processed using a MINC toolkit with SUVRs calculated for 57 regions of interest (ROIs) normalized to cerebellar grey matter (^{18}F-Florbetapir) and pons (^{18}F-FDG)
- SUVRs used to train RFs and K-means clustering

IMAGE PROCESSING PIPELINE

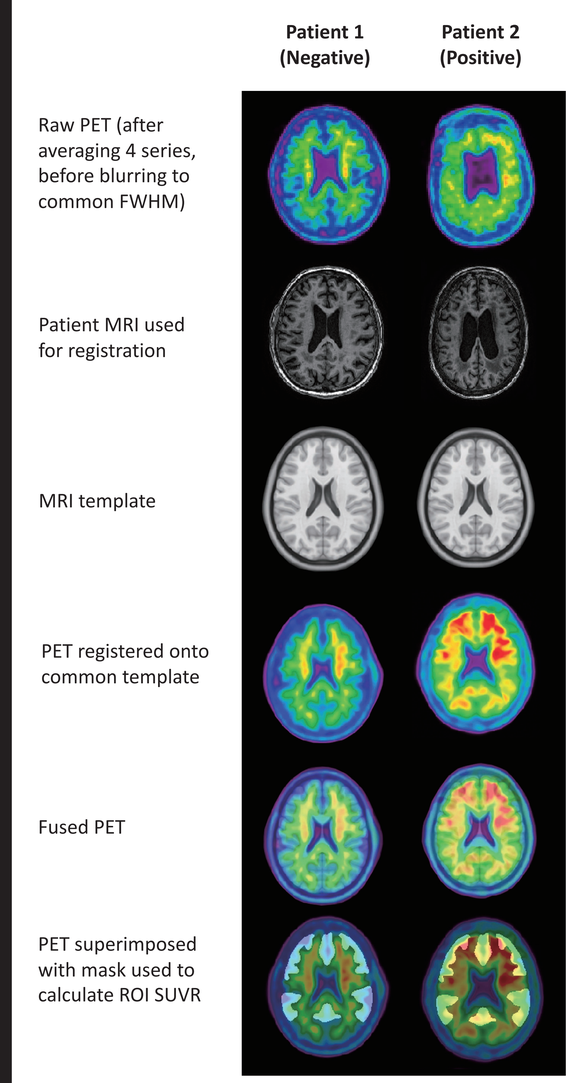

SUVR = 1.073 1.672

SUVRs calculated for 57 ROIs, normalized to cerebellar grey matter (^{18}F-Florbetapir) or pons (^{18}F-FDG)

	Patient 1	Patient 2		Patient 1	Patient 2
Jack mask	1.073	1.672			
L angular gyrus	0.882	1.488	R angular gyrus	0.968	1.479
L anterior cingulate gyrus	0.980	1.808	R anterior cingulate gyrus	0.948	1.887
L caudate	0.688	0.383	R caudate	0.782	0.425
L cuneus	0.867	1.077	R cuneus	0.990	1.148
L fusiform gyrus	1.101	1.588	R fusiform gyrus	1.138	1.532
L gyrus rectus	0.905	1.452	R gyrus rectus	0.912	1.481
L hippocampus	1.003	1.116	R hippocampus	0.998	0.936
L inferior frontal gyrus	0.833	1.478	R inferior frontal gyrus	0.870	1.486
L inferior occipital gyrus	1.125	1.640	R inferior occipital gyrus	1.061	1.564
L inferior temporal gyrus	1.105	1.569	R inferior temporal gyrus	1.113	1.637
L insular cortex	0.866	1.332	R insular cortex	0.790	1.241
L lateral orbitofrontal gyrus	1.015	1.533	R lateral orbitofrontal gyrus	1.140	1.464
L lingual gyrus	1.041	1.364	R lingual gyrus	1.014	1.300
L middle frontal gyrus	0.986	1.462	R middle frontal gyrus	1.013	1.509
L middle occipital gyrus	1.025	1.223	R middle occipital gyrus	0.992	1.320
L middle orbitofrontal gyrus	1.151	1.790	R middle orbitofrontal gyrus	1.217	1.659
L middle temporal gyrus	0.968	1.505	R middle temporal gyrus	0.960	1.516
L parahippocampal gyrus	1.025	1.168	R parahippocampal gyrus	0.944	1.011
L posterior cingulate	1.021	2.011	R posterior cingulate	1.065	1.967
L postcentral gyrus	0.914	1.457	R postcentral gyrus	0.881	1.267
L precentral gyrus	1.029	1.454	R precentral gyrus	0.936	1.321
L precuneus	0.938	1.874	R precuneus	0.970	1.828
L putamen	1.199	1.519	R putamen	1.377	1.579
L superior frontal gyrus	1.034	1.623	R superior frontal gyrus	1.024	1.705
L superior occipital gyrus	0.897	1.170	R superior occipital gyrus	0.937	1.067
L superior parietal gyrus	1.048	1.464	R superior parietal gyrus	0.921	1.201
L superior temporal gyrus	0.846	1.211	R superior temporal gyrus	0.767	1.041
L supramarginal gyrus	0.835	1.407	R supramarginal gyrus	0.844	1.135

SIMPLE MACHINE LEARNING

	SUVmax	diam	sex	age	height	weight	clinical finding
1	7.0	3.2	M	61	177	75	POS
2	2.6	2.1	M	70	165	76	NEG
3	6.2	2.3	F	71	162	70	POS
4	1.1	4.0	M	83	185	81	NEG
5	5.0	1.5	F	60	148	68	NEG
6	4.1	7.0	F	63	167	85	POS
7	3.4	7.9	F	59	156	64	NEG
8	6.9	6.5	F	88	146	57	POS
9	1.8	3.5	F	91	125	53	NEG
10	3.3	4.0	M	71	173	83	POS

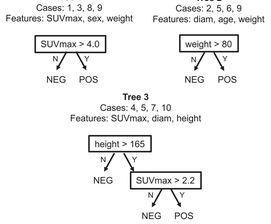

Illustration of RF with 3 trees. Initial data (left) used to train RF to correctly classify clinical finding of new cases using 6 features.

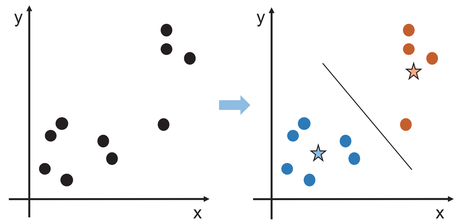

Illustration of K-means clustering with K = 2. Initial data (left) has two measurements in dimensions x and y. Data is clustered (right) into blue and orange groups, with stars showing centers of mass.

RESULTS

Supervised and unsupervised ML had similar classification accuracy (~85%) for ^{18}F-Florbetapir PET with clinical interpretation as the gold standard.

Most common ROIs used for classification were:

1) Left posterior cingulate
2) Left precuneus
3) Left middle frontal gyrus

While associations of FDG uptake with pvWMH were complex, amyloid deposition was higher in subjects with moderate-severe pvWMH at baseline and accumulated faster at 2-years in subjects with moderate-severe pvWMH than in matched ADNI cohorts

CONCLUSIONS

Results suggest amyloid deposition and accumulation are associated with pvWMH load

REFERENCE / ACKNOWLEDGMENTS

C.F. Uribe, S. Mathotaarachchi, V. Gaudet, K.C. Smith, P. Rosa-Neto, F. Bénard, S.E. Black, and K. Zukotynski, "Machine Learning in Nuclear Medicine: Part 1–Introduction," *J Nucl Med.* 2019;60(4):451-458.

We gratefully recognize the support of AVID Radiopharmaceuticals for their contribution of the AV-45 radioligand, and CIHR MITNEC-C6 (mitnec.org) for the study data. Also, we wish to acknowledge S. Mathotaarachchi and P. Rosa-Neto for their help with the image processing pipeline.

Matched data collection and sharing for this project was funded in part by the Alzheimer's Disease Neuroimaging Initiative (ADNI) (National Institutes of Health Grant U01 AG024904) and DOD ADNI (Department of Defense award number W81XWH-12-2-0012).